The expected performance of nulling at the VLTI down to 5 mas

Romain Laugier, Denis Defrère, Alexis Matter, Simon Gross, Benjamin Courtney-Barrer, et al.

Romain Laugier, Denis Defrère, Alexis Matter, Simon Gross, Benjamin Courtney-Barrer, Felix Dannert, Julien Woillez, Olivier Absil, Colin Dandumont, "The expected performance of nulling at the VLTI down to 5 mas," Proc. SPIE 12183, Optical and Infrared Interferometry and Imaging VIII, 1218321 (26 August 2022); doi: 10.1117/12.2629292

SPIE.

Event: SPIE Astronomical Telescopes + Instrumentation, 2022, Montréal, Québec, Canada

The expected performance of nulling at the VLTI down to 5 mas

Romain Laugier[a], Denis Defrère[a], Alexis Matter[b], Simon Gross[c], Benjamin Courtney-Barrer[d,g], Felix Dannert[e], Julien Woillez[d], Olivier Absil[f], and Colin Dandumont[f]

[a]Institute of Astronomy, KULeuven, 200D Celestijnenlaan, Leuven, Belgium
[b]Université Côte d'Azur, Observatoire de la Côte d'Azur, Laboratoire Lagrange, CNRS, France
[c]Macquarie University, Australia
[d]European Southern Observatory
[e]ETH Zurich, Switzerland
[f]University of Liège, Belgium
[g]Australian National University, Canberra, Australia

ABSTRACT

While VLTI offers the recombination of four 8-m telescopes with baselines of more than 100m, it has never hosted a dedicated high-contrast nulling beam-combiner. The SCIFY project aims to design, build and commission Hi-5, the first nulling beam-combiner of the VLTI, optimized for the detection and characterization of young giant exoplanets near the snow line, with spectroscopy up to R=2000 in the L' band. It will make use of advanced four-beam nulling combination schemes, like double-Bracewell and kernel-nulling implemented in a single-mode photonic device to produce differential nulled outputs with self-calibrating properties. In the wavelength range of interest, both instrumental errors and background noise are significant. In order to estimate the practical performance of these different configurations in the presence of instrumental errors and further optimize the instrumental design, we have developed SCIFYsim. SCIFYsim is an end-to-end simulator geared towards single-mode beam combiners with of a wide variety of instrumental errors, like optical path difference residuals from fringe tracking, wavefront error at the injection, longitudinal dispersion, chromaticity of the combiner chip, and more. In order to evaluate the performance of the combined spectral channels, we use statistical tests based on likelihood ratios, and account for the covariance in the data. In this paper, we present the expected performance of Hi-5 with a few examples and discuss the main technical limitations to reach the contrast required to image young giant exoplanets.

Keywords: Nulling interferometry, simulator, kernel-nulling, VLTI, Hi-5, Photonics, Double-Bracewell

1. INTRODUCTION

Direct detection of giant planets inside the snow line of nearby young stars is very important for understanding planetary formation. Long-baseline interferometry is the only practical way to probe such angular separations. Hi-5[1] is a module of the new ASGARD visitor instrument of the VLTI producing a nulling combination with spectroscopy up to $R \approx 2000$ from 3.5 to 4.0 µm. Here we report our method for evaluating the performance of this module.

2. DIFFERENTIAL NULLING

Nulling interferometry is an approach that may be directly compared to coronagraphy. A nulling beam-combiner accomplishes the same function for interferometry as coronagraph does for imaging. It optically separates the the on-axis starlight into a different channel in order to access off-axis light without the limitation of the photon

Further author information: (Send correspondence to R. Laugier)
R.Laugier.: E-mail: romain.laugier@kuleuven.be, Telephone: +33 (0)6 82 91 47 05

Optical and Infrared Interferometry and Imaging VIII, edited by Antoine Mérand, Stephanie Sallum, Joel Sanchez-Bermudez,
Proc. of SPIE Vol. 12183, 1218321 · © 2022 SPIE · 0277-786X · doi: 10.1117/12.2629292

noise. Therefore a nuller does not measure the full fringe visibility but a different observable quantity constructed from the light in the supposedly *dark* outputs.

Just as with coronagraphy, where the contribution of the photon noise in the wings of the stellar image is removed and the speckle noise becomes the dominant error source, here as well, a variable leakage light pollutes the outputs in the form of a complicated instrumental noise term.[2]

The staged combination used here, referred to as double Bracewell combiner[3] produces two dark outputs rather than one. The signal produced by an off-axis source on these two outputs quickly decorrelates, whereas the leakage light is quite correlated. This gives the opportunity to produce a differential output for which the first order errors and most second order error terms cancel-out, providing improved precision and sensitivity to higher-contrast companions.

3. EVALUATION OF PERFORMANCE

Despite this reduction, the instrumental errors remain a dominant term for a large part of the scientific goal. Furthermore, its contribution is correlated over the different spectral bins. In order to provide a meaningful statistical detection limit, its covariance matrix must be estimated. For this, we developed the end-to-end simulator for this module, and used it in semi-analytical evaluation of the errors.

SCIFYsim[*] is designed to provide realistic outputs simulating real observing sessions. It includes different noise sources that can be evaluated separately.

3.1 Time-varying noises

This includes the errors effecting the complex amplitude of the input beams to the combiner.

Fringe-tracking error coming from imperfect correction of atmospheric turbulence by the fringe tracker dominate the input phase error. These are currently indexed on the power spectrum of the GRAVITY fringe tracker, producing 100nm RMS of differential piston errors. Hi-5 will eventually benefit from fringe tracking by the Heimdallr module of Asgard.

Injection fluctuation are produced by scanning a wavefront screen in front of the instruments pupil and computing the injection integral for the instrument waveguides. The resulting errors in phase and amplitude are both taken into account in the combination.

3.2 Static noises

In addition to the dynamic perturbations, static errors are also taken into account. The thermal light from the sky and warm optical train are dominating the leakage light and produce photon noise. Readout noise is also a limitation at the higher spectral resolution.

A crucial aspect of the performance budget is grouped under the name of combiner imperfections, encompassing the deviations from the ideal combination schemes with equal contribution of the four inputs phased by four steps of $\pi/2$. As highlighted in previous works on kernel nulling,[4] the symmetry of the two dark combination diagrams is important to provide the stability in the differential observables at the different wavelengths. Such chromatic aberrations are examined in plots such as Figure 1, which uses one color per input, one diagram per output, and gray to represent the resulting complex combination for an on-axis source.

Variable thickness ZnSe plates[5] are then used to adjust dispersion to compensate the chromatic behavior of the imperfect component built with imperfect organs, such as measured by Tepper et al.[6]

3.3 Other sources

Later versions of the simulator will include simulation and imperfect compensation of the longitudinal atmospheric dispersion and their effect; and simulation of the effects of transverse atmospheric dispersion on the injection. Dynamical effects to the optical paths caused by dispersion (water vapor seeing) will also be added in a later stage.

[*]https://github.com/rlaugier/scifysim

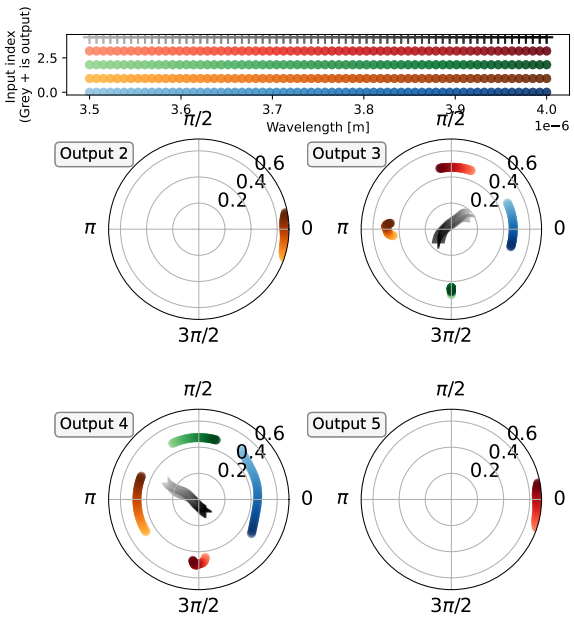

Figure 1. Complex matrix plot across the wavelength range of 3.5-4.0µm. Each diagram represent an output, each color corresponds to an input, except for gray which is complex combination of all inputs. In output 1 and 2, the distance from each gray + to the center translates the depth of the null, but the relative symmetry of the dots position at each wavelength is also important to reduce instrumental noise.

4. SCALING OF ERRORS

The mean leakage light scales with the star luminosity, but is a small contributor to the overall photon noise which is dominated by background thermal light. Here, photon noise is uncorrelated across the spectral channels.

The instrumental noise (fluctuation of the leakage light) in the differential output tends toward a Gaussian distribution when the instrument combination tends toward the ideal nominal combination. Monte-Carlo simulations are used to evaluate its covariance matrix for a given detector integration time and spectral resolution.

The observing sequence over a 6h observing session (50% overhead) is average over a number (typically 20) of temporal chunks, and the covariance matrix is scaled consequently. The observables values collected for each chunk are concatenated into a single vector, for which the covariance matrix $\mathbf{\Sigma}$ is block diagonal, as illustrated in Figure 2.

The correlations on the errors are taken into account using a whitening matrix $\mathbf{W}$ as has been used for kernel-phases,[7] which can be obtained from the covariance matrix.

5. DETECTION TEST

The transmission offered by the array of apertures projected on the plane orthogonal to the line of sight varies over this observing session, as illustrated by a schematic of the UV coverage showed in Figure 3.

This information gathered can be combined into detection tests, translating these values into sensitivity threshold for given risk of error, like a detection probability P_{det}, and the false alarm rate P_{FA}. We give the performance for a $P_{FA} = 0.01$ and $P_{det} = 0.9$. Following the example of set by Ceau,[7] we define a lower and upper bound for optimal testing, depending on how the signature of interest is defined.

A completely unknown signature corresponding to anything that deviates from the expected distribution leads to the energy detector test T_E, which is a lower bound to the sensitivity.

A perfectly known signature corresponding to a confirmation test for presence of signature detected by other means produces a Neyman-Pearson test T_{NP}, which is demonstrably the upper bound to the sensitivity.

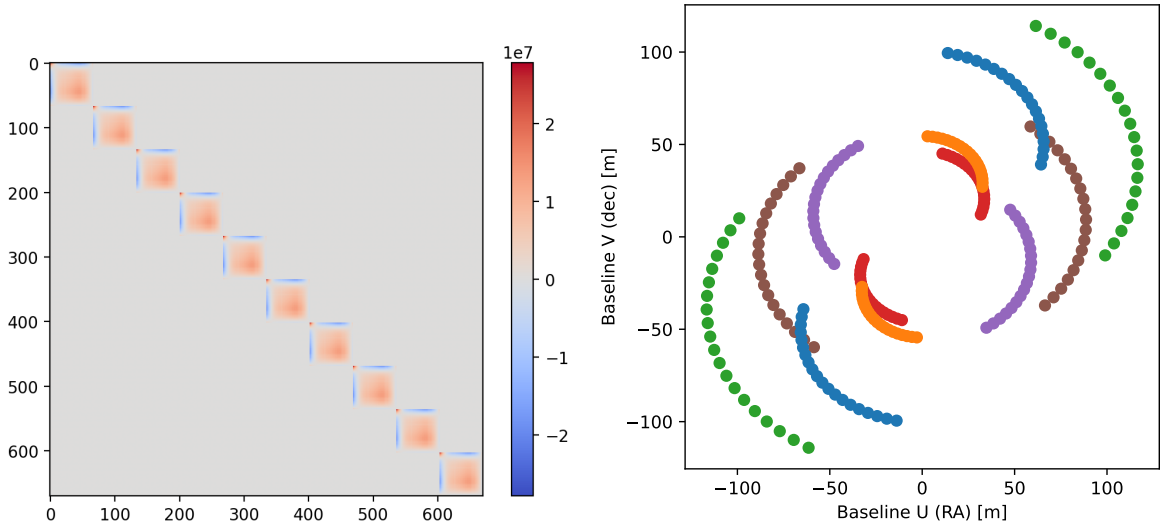

Figure 2. Left: An example of concatenated covariance matrix (only ten chunks here, fore readability). Each block on the diagonal is the covariance of the mean observables on a given temporal chunk of the session. Right: The UV coveraged obtained for the 20 chunks of an observing session for a typical -50 dec. target.

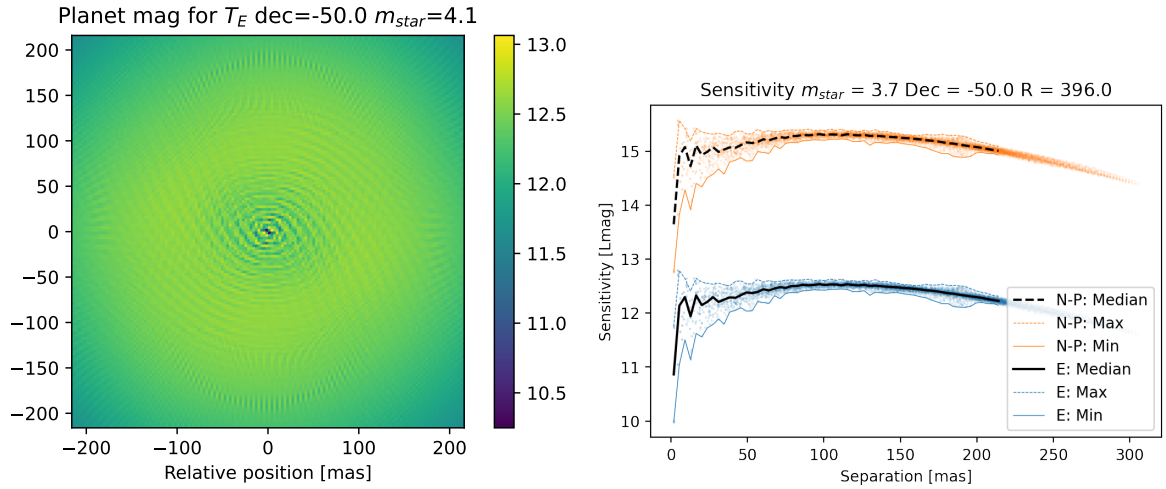

Figure 3. Left: The detection map obtained for the energy detector test at a spectral resolution $R \approx 400$. Right: Translation of the map into one-dimension graph as a cloud of dots and median curve.

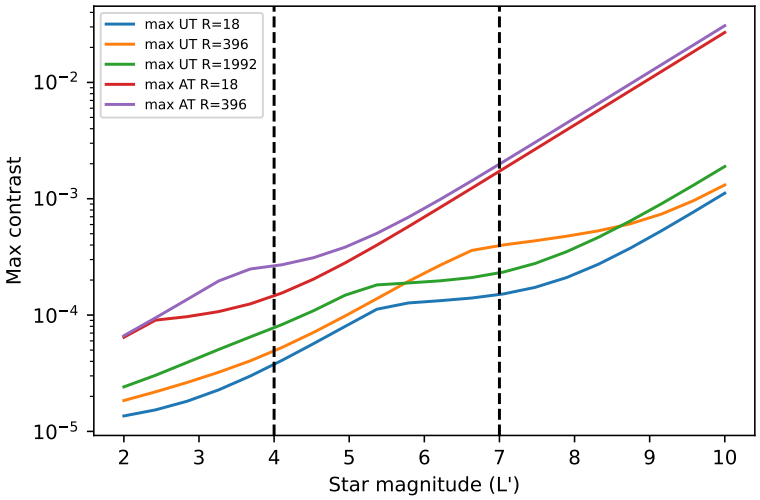

Figure 4. Contrast sensitivity as a function of star magnitude for different instrument modes on the best pixel of the map. The dashed black lines indicate a transition regime between background dominated noise and instrumental noise dominated regime, both for UTs and ATs.

A practical test for an off-axis point source would offer a sensitivity somewhere in between the two. The sensitivity maps are translated from the pixel data into a one-dimensional graph through median, as illustrated in Figure 3.

Thanks to the semi-analytic scaling of errors, these maps can be declined as a function of star magnitude. The sensitivity of the best pixel (and the 95 percentile pixel) can be showed as a function of stellar magnitude, and displayed in contrast. The more conservative T_E test is used here. These plots are display in Figure 4.

On the fainter stars, the smallest separation first peak is a most sensitive region, as indicated by an offset between (3-4 for ATs and 6-7 for UTs) the observations are background dominated. On the brighter stars, the instrumental noise becomes dominant, reducing the sensitivity of this first peak, and the maximum is further afield.

These contrast values go down to 10^{-4} - 10^{-5}, which is sufficient to detect hot giant planets around nearby stars, and obtain spectral information.

6. CONCLUSION

We have proposed a prediction of the performance of the coming nulling-interferometer ASGARD/Hi-5 for the VLTI. Due to the complex nature of instrumental noise, we have used Monte-Carlo simulations to characterize the effect of different sources of noise, and proposed a data reduction scheme that allows for rigorous statistical hypothesis detection tests. The sensitivity of those tests is given here for 1% false-alarm rate for a broad range of stellar magnitudes.

Further work will include additional sources of uncertainties, such as the varying atmospheric dispersion, water-vapor seeing and polarization errors. Evaluation of the capability for spectral and astrometric characterization will also be an active topic in the near future.

ACKNOWLEDGMENTS

SCIFY has received funding from the European Research Council (ERC) under the European Union's Horizon 2020 research and innovation program (grant agreement CoG - 866070).

REFERENCES

[1] Defrère, D., Absil, O., Berger, J. P., Boulet, T., Danchi, W. C., Ertel, S., Gallenne, A., Hénault, F., Hinz, P., Huby, E., Ireland, M., Kraus, S., Labadie, L., Le Bouquin, J. B., Martin, G., Matter, A., Mérand, A., Mennesson, B., Minardi, S., Monnier, J. D., Norris, B., de Xivry, G. O., Pedretti, E., Pott, J. U., Reggiani, M., Serabyn, E., Surdej, J., Tristram, K. R., and Woillez, J., "The path towards high-contrast imaging with the VLTI: The Hi-5 project," *Experimental Astronomy* **46**(3), 475–495 (2018).

[2] Lay, O. P., "Systematic errors in nulling interferometers," *Applied Optics* **43**(33), 6100–6123 (2004).

[3] Angel, J. R. P. and Woolf, N. J., "An Imaging Nulling Interferometer to Study Extrasolar Planets," *The Astrophysical Journal* **475**(1), 373–379 (1997).

[4] Laugier, R., Cvetojevic, N., and Martinache, F., "Kernel nullers for an arbitrary number of apertures," *Astronomy and Astrophysics* **642**, A202 (2020).

[5] Koresko, C., Mennesson, B., Serabyn, E., Colavita, M. M., Akeson, R. L., and Swain, M. R., "Longitudinal dispersion control for the Keck Interferometer Nuller," in [*Proc of SPIE*], **4838** (2003).

[6] Tepper, J., Labadie, L., Diener, R., Minardi, S., Pott, J. U., Thomson, R., and Nolte, S., "Integrated optics prototype beam combiner for long baseline interferometry in the L and M bands," *arXiv* **66** (2017).

[7] Ceau, A., Mary, D., Greenbaum, A., Martinache, F., Sivaramakrishnan, A., Laugier, R., and N'Diaye, M., "Kernel-phase detection limits: Hypothesis testing and the example of JWST NIRISS full-pupil images," *Astronomy and Astrophysics* **630**, A120 (2019).